Dynamical coupling effects in the vibrational excitation of H_2 and N_2 colliding with positrons

F. A. Gianturco* and T. Mukherjee†
Department of Chemistry, The University of Rome, Città Universitaria, 00185 Rome, Italy
(Received 8 July 1996)

The coupling between angular momenta during low-energy collisions of slow positrons as projectiles on simple diatomics like H_2 and N_2 is analyzed from the point of view of its effect on vibrationally inelastic processes and on possible decoupling schemes that can help to simplify calculations. It is found that the strong decoupling between rotational and vibrational degrees of freedom implied by the well-known infinite-order-sudden approximation (here used within the vibrational close-coupling-rotational-infinite-order-sudden scheme discussed below) is not valid for positron scattering at low collision energies in spite of its low excitation efficiency for the vibrational degrees of freedom of the target molecules. [S1050-2947(97)06201-X]

PACS number(s): 34.90.+q, 34.10.+x

I. INTRODUCTION

The measurement of total inelastic-scattering cross sections for positrons is currently one of the major thrusts in the experimental study of positron collisions. Ten years ago, for instance, our only information on the relative size of inelastic cross sections, over a fairly restricted range of energies, had been deduced from positronium Ps formation fractions in dense gases measured in positron lifetime experiments [1]. The first direct observations of inelastic-scattering processes were made by identifying the scattered positrons in the measurement of their time of flight [2,3]. More recently, however, because of the advances in positron beam technology, and of the attendant increase by two or three orders of magnitude of beam intensities that can be used, the direct measurements of cross sections for Ps formation [4] and atomic [5] and molecular [6] ionization have been made possible by sensitive nontiming methods. The very recent surge of interest on positron use for medical imaging has also markedly increased the range of possible applications of the more intense sources.

On the other hand, much work still remains to be done on the very wide variety of inelastic processes that can be observed in atomic and molecular systems even below the threshold of Ps formation. For example, experimental data on positron impact excitation of specific electronic states is still sparse and it is almost nonexistent for excitations of molecular rotational and vibrational degrees of freedom. No measurements can be found on molecular dissociation by positrons still. Furthermore, with the advent of intense positron sources and the production of intense positron beams it should become possible to measure differential inelastic cross sections with high-energy resolution. Until this prediction becomes reality, however, we still have to rely on computational modeling of many of the above processes and on the general shape and values of theoretical inelastic cross sections, integral and differential, in order to start to discern patterns of behavior across series of atomic and molecular targets.

In particular, even if one limits the analysis to the low-energy range below Ps formation and to situations where the molecular electronic degrees of freedom are not involved in the excitation processes, the wealth of possible transitions that can occur between rotational and vibrational levels of molecular targets can still provide a formidable challenge for the theoretical models and have actually been carried out only for a very limited set of examples [7–9]. An alternative theoretical scheme has been pursued for the H_2 molecule by Armour, Baker, and Plummer [10].

In order to extend at least the computational options that can be open to exploratory studies directed at guiding experimental analysis, we study in the present work some of the possible dynamical approximations that can be used to analyze vibrational excitation processes in positron collisions with simple targets like H_2 and N_2. We have recently carried out a similar study for rotational excitations in e^+-CO_2 collisional processes [9] and compared it with available results for electron-CO_2 inelastic collisions, thereby discovering marked effects on inelasticity that are induced by simply changing the sign of the projectile charge, as already surmized by the theoretical studies on elastic cross sections [11].

In Sec. II we report in detail our computational model while the actual results are summarized in Sec. III. Our conclusions are finally discussed in Sec. IV.

II. THEORETICAL MODEL

To describe the scattering of positrons by a vibrating molecule in its electronic ground state one has to solve the familiar Schrödinger equation

$$(\mathfrak{H}-E)\Psi=0 \tag{1}$$

subject to the usual scattering boundary conditions. Here $\mathfrak{H}$ and Ψ are the total Hamiltonian and the total wave function of the positron-molecule system. The expansion of this Hamiltonian and of the wave function in terms of the molecular Hamiltonian and of the molecular eigenfunctions depends on the coupling scheme one decides to employ. In a

*Author to whom correspondence should be addressed. FAX: 39-6-49913305. Electronic address: FAGIANT@CASPUR.IT
†On leave from Department of Theoretical Physics, Indian Association for the Cultivation of Science, Jadavpur, Calcutta 32, India.

 © 1997 The American Physical Society

body-fixed (BF) vibrational close-coupling (BFVCC) approximation the total Hamiltonian can be written as [12]

$$\mathfrak{H}^{\mathrm{BFVCC}}=\mathfrak{H}(\mathbf{r}_p)+\mathfrak{H}_{\mathrm{el}}(\mathbf{r}_e)+\mathfrak{H}_{\mathrm{vib}}(\mathbf{R})+V_{\text{p-mol}}(\mathbf{r}_p,\mathbf{r}_e,\mathbf{R}), \tag{2}$$

where $\mathbf{r}_p$ is the positron coordinate measured from the center of mass of the system, $\mathbf{r}_e$ collectively denotes the molecular electronic coordinates, and $\mathbf{R}$ is the internuclear set of coordinates of the molecule. $\mathfrak{H}(\mathbf{r}_p)$ is the kinetic-energy operator for the impinging positron, $\mathfrak{H}_{\mathrm{vib}}(\mathbf{R})$ and $\mathfrak{H}_{\mathrm{el}}(\mathbf{r}_e)$ are the vibrational and electronic Hamiltonians, respectively.

$V_{\text{p-mol}}(\mathbf{r}_p,\mathbf{r}_e,\mathbf{R})$ represents the positron-molecule interaction. It is to be noted here that in the BFVCC scheme the rotational part $\mathfrak{H}_{\mathrm{rot}}(\hat{\mathbf{R}})$ from the full Hamiltonian is neglected because of the BF frame that is being employed. The wave function of the BFVCC representation is now expanded as

$$\Psi^{\mathrm{BVCC}}=\chi_0(\mathbf{r}_e|\mathbf{R})\sum_{\nu,l}\phi_\nu(\mathbf{R})u^{\Lambda}_{\nu l,\nu_0 l_0}(r_p)(r_p^{-1})Y_{l\Lambda}(\hat{\mathbf{r}}_p), \tag{3}$$

where $\chi_0(\mathbf{r}_e|\mathbf{R})$ is the ground-state electronic wave function parametrically dependent on $\mathbf{R}$, ϕ_ν is the vibrational wave function of the molecule, and ν labels the vibrational quantum number. $Y_{l\Lambda}(\hat{\mathbf{r}}_p)$ denotes the angular part of the positron wave function, l is the orbital angular momentum of the positron, and Λ is the projection of l along the internuclear axis $\Lambda=\boldsymbol{l}\cdot\hat{\mathbf{R}}$. In the BFVCC scheme this quantity is a good quantum number (constant of motion). $u^{\Lambda}_{\nu_l,\nu_0 l_0}(r_p)$ is the radial part of the positron wave function, where $(\nu_0 l_0)$ denotes the particular initial channel that has been selected.

Using now Eqs. (2) and (3) in the Schrödinger equation (1) one gets the corresponding BFVCC coupled differential equations

$$\left\{\frac{d^2}{dr_p^2}-\frac{l(l+1)}{r_p^2}+k_\nu^2\right\}u^{\Lambda}_{\nu l,\nu_0 l_0}(r_p) =2\sum_{\nu' l'}V^{\Lambda}_{\nu l,\nu' ,l'}(r_p)\mathbf{u}^{\Lambda}_{\nu' l',\nu_0 l_0}(r_p) \tag{4}$$

with

$$V^{\Lambda}_{\nu l,\nu' l'}(r_p)=\sum_{\lambda}\langle\phi_\nu(\mathbf{R})|V_\lambda(r_p|\mathbf{R})|\phi_{\nu'}(\mathbf{R})\rangle g^{\Lambda}_{\lambda}(ll'), \tag{5a}$$

$$g^{\Lambda}_{\lambda}(ll')=\left\{\frac{2l'+1}{2l+1}\right\}^{1/2}C\begin{pmatrix}\lambda & l' & l\\ 0 & \Lambda & \Lambda\end{pmatrix}C\begin{pmatrix}\lambda & l' & l\\ 0 & 0 & 0\end{pmatrix}, \tag{5b}$$

and

$$k_\nu^2=2(E-\epsilon_\nu), \tag{5c}$$

ϵ_ν being the energy of the νth vibrational state. V_λ is obtained from the following expression:

$$\langle\chi_0(\mathbf{r}_e|\mathbf{R})|V_{\text{p-mol}}(\mathbf{r}_p,\mathbf{r}_e,\mathbf{R})|\chi_0(\mathbf{r}_e|\mathbf{R})\rangle =\sum_{\lambda}V_\lambda(r_p|\mathbf{R})P_\lambda(\hat{\mathbf{r}}_p\cdot\hat{\mathbf{R}}) \tag{6}$$

and the C's of Eq. (5b) are the usual Clebsh-Gordan coefficients. The vibrational wave functions of the molecule can be obtained first by solving the following differential equations:

$$\left\{\frac{d^2}{d\mathbf{R}^2}+2\mu[\epsilon_\nu-\epsilon(\mathbf{R})]\right\}\phi_\nu(\mathbf{R})=0, \tag{7}$$

where μ is the reduced mass of the molecule and $\epsilon(\mathbf{R})$ is electronic energy providing the potential that supports the different nuclear geometries as vibrational bound states. The solution of the coupled Equation (4) subject to the usual asymptotic boundary condition gives the T matrix $T^{\Lambda}_{\nu l,\nu_0 l_0}$ and from it we can get the partial integral vibrational excitation cross section using the following expression:

$$\sigma(\nu_0\rightarrow\nu)=\frac{\pi}{k_\nu^2}\sum_{\Lambda}\sum_{ll_0}|T^{\Lambda}_{\nu l,\nu_0 l_0}|^2. \tag{8}$$

When the energy of the incoming positron is such that the energy spacing between rotational levels is only a small fraction of the total energy, then the molecule is considered to be nonrotating and the BFVCC scattering cross sections can be considered to be exact. We should also point out here that, even if there are resonance phenomena present in collision processes, this method can still give reasonably good results [13]. Equation (4) for the BFVCC method states that the vibrational motion of the molecule and the angular momentum of the positron are coupled via the $V^{\Lambda}_{\nu l,\nu' l'}(r_p)$. It therefore becomes less transparent to understand which of the coupling, either the vibrational or the one via the angular momentum, is more effective in driving a particular scattering process. The possible understanding of the relative importance of the different couplings during the dynamics can be achieved more directly if one introduces an approximate scheme that has been used quite extensively for the local interactions in atom-molecule collisions [14–16] and then compares the final results by using both this latter method and the BFVCC coupling scheme. This approximate coupling scheme goes under the name of rotational-infinite-order-sudden (IOS) approximation [14]. It essentially assumes that the relative velocity between target and projectile and the nature of their interaction allows one to make the following dynamical assumptions: (i) that the energy losses during inelastic collisions produce final wave vectors that are rather close in magnitude to the initial wave vectors [the energy sudden (ES) approximation], and further that (ii) the recoupling of relative angular momenta during collisions does not occur and therefore the centrifugal momentum $\hat{l}$ is conserved during each collision. This is the centrifugal sudden (CS) approximation [15]. The corresponding RIOS Hamiltonian can now be written as follows:

$$\mathfrak{H}^{\mathrm{RIOS}} = H(\mathbf{r}_p) + \frac{\overline{l(l+1)}}{2r_p^2} + \frac{\overline{j(j+1)}}{2I} + \mathfrak{H}_{\mathrm{el}}(\mathbf{r}_e) + V_{\text{p-mol}}(\mathbf{r}_p, \mathbf{r}_e, \mathbf{R}), \tag{9}$$

where $\overline{l}$ and $\overline{j}$ correspond to initial, arbitrary choices for the eigenvalues of $\hat{l}$ and $\hat{j}$.

The inclusion of the vibrational hamiltonian $\mathfrak{H}_{\mathrm{vib}}(\mathbf{R})$, as in Eq. (2), will yield the further approximation called VCC-RIOS [17]. The latter rewrites the BF wave function in the following form:

$$\Psi^{\text{BF-VCCRIOS}} = \chi_0(\mathbf{r}_e|\mathbf{R}) \sum_{\nu} \phi_\nu(\mathbf{R}) u^{\overline{l}}_{\nu,\nu_0}(r_p|\hat{\mathbf{r}}_p) \times (r_p^{-1}) Y_{l\Lambda}(\hat{\mathbf{r}}_p), \tag{10}$$

where the as yet unknown, radial coefficients u^{l}_{ν,ν_0} are now parametrically dependent on the relative orientation of the impinging positron with respect to the fixed molecular axis of the diatomic target [16]. This can be explicitly related to the BFVCC radial coefficients of Eq. (3) by writing

$$u^{\wedge}_{\nu',l',\nu_0 l_0}(r_p) = \langle l'\wedge | u^{l_0}_{\nu'}(r_p|\hat{\mathbf{r}}_p) | l_0\wedge \rangle, \tag{11}$$

where l_0 is now the initial value of the positron relative angular momentum and it is equivalent to the constant value $\tilde{l}$ (an arbitrary choice) required by the CS part of the IOS approximation and defined in Eq. (9). In other words, the angular averaging indicated by Eq. (11) produces the radial functions of the BFVCC equations using the solutions of the scattering problem at fixed relative orientations, thereby including the $(l_0 l')$ coupling only after the dynamics has been solved for a set of separate, adiabatically decoupled angular momenta. This approximation therefore suggests that a more simplified form of the BFVCC solutions could be achieved by introducing an adiabatic angular momentum coupling scheme (AAMCS) on top of the more exact BFVCC expansion of Eq. (3). This means that in the new RIOS approximation the BFVCC form of the positron wave function $u^{\wedge}_{\nu_l,\nu_0 l_0}(\mathbf{r}_p)$ is separated in terms of a part that depends on the relative value of the Jacobi angle of the positron with the molecular bond $\mathbf{R}$, i.e., a fixed-angle function $u^{l_0}_{\nu\nu_0}(r_p|\hat{\mathbf{r}}_p)$ and an angular part $Y_{l\wedge}(\hat{\mathbf{r}}_p)$. In more precise terms this decoupling can be expressed via the angular averaging given in [Eq. (11)].

Using this expression in Eq. (3) for the BFVCC total wave function, one therefore gets the BFVCC-AAMCS total wave function defined now as in Eq. (10) which, for a diatomic molecular target, reads

$$\psi^{\text{BFVCC-AAMCS}}_{l_0} = \chi_0(\mathbf{r}_e|\mathbf{R}) \sum_{\nu} \phi_\nu(\mathbf{R}) u^{l_0}_{\nu,\nu_0}(r_p|\hat{\mathbf{r}}_p) \times (r_p)^{-1} Y_{l_0\wedge}(\hat{\mathbf{r}}_p). \tag{12}$$

Here we have considered that, under the fixed nuclei approximation, the sum $\Sigma_l |l\wedge\rangle\langle l\wedge| = 1$. The additional acronym now stands for adiabatic angular-momentum coupling (AAMC) because of the fixed value l_0 implied by the CS approximation discussed before.

Using the BFVCC Hamiltonian [Eqs. (1) and (12)] one now gets the BFVCC-AAMC's new approximate set of coupled differential equations:

$$\left\{ \frac{d^2}{dr_p^2} - \frac{l_0(l_0+1)}{r_p^2} + k_\nu^2 \right\} u^{l_0}_{\nu,\nu_0}(r_p|\hat{\mathbf{r}}_p) = 2 \sum_{\nu'} V^{\wedge}_{\nu\nu'}(r_p|\hat{\mathbf{r}}_p) u^{l_0}_{\nu}(r_p|\hat{\mathbf{r}}_p) \tag{13}$$

with

$$V_{\nu\nu'}(r_p|\hat{\mathbf{r}}_p) = \sum_{\lambda} \langle \phi_\nu(\mathbf{R}) | V_\lambda(\mathbf{r}_p|\mathbf{R}) | \phi_{\nu'}(\mathbf{R}) \rangle P_\lambda(\hat{\mathbf{r}}_p), \tag{14}$$

where the coupling now acts at each fixed relative orientation, $\hat{\mathbf{r}}_p$. The asymptotic solutions of the BFVCC-AAMC coupled equations (13) for the positron wave function $u^{l_0}_{\nu' \nu_0}(r_p|\hat{\mathbf{r}}_p)$ give the parameter-dependent (fixed-angle) T-matrix element $T^{l_0}_{\nu',\nu_0}(\hat{\mathbf{r}}_p)$. The previous BFVCC T-matrix elements can now be obtained under the BFVCC-AAMC approximation by using the following relation:

$$T^{\wedge}_{\nu l,\nu_0 l_0} = \langle l\wedge | T^{l_0}_{\nu,\nu_0} | l_0\wedge \rangle. \tag{15}$$

Equation (15) is obtained by combining the asymptotic parts of the BFVCC and of the BFVCC-AAMC's positron wave functions.

To understand more clearly the difference between the BFVCC and BFVCC-AAMC's method one can further proceed as follows. Let us consider Eq. (15) and expand the T-matrix element $T^{l_0}_{\nu,\nu_0}(\hat{\mathbf{r}}_p)$ as

$$T^{l_0}_{\nu,\nu_0}(\hat{\mathbf{r}}_p) = \sum_L h^{l_0}_{\nu,\nu_0,L} P_L(\hat{\mathbf{r}}_p). \tag{16}$$

Then we get

$$T^{\wedge}_{\nu_l,\nu_0 l_0} = \sum_L \langle l\wedge | h^{l_0}_{\nu,\nu_0,L} P_L(\hat{\mathbf{r}}_p) | l_0\wedge \rangle = \sum_L h^{l_0}_{\nu,\nu_0} g^{\wedge}_L(l l_0), \tag{17}$$

where $g_L(l l_0)$ is defined in Eq. (5b).

The BFVCC coupled equations (4) and (5) have shown that the orbital angular momenta of the positron motion are coupled through the angular part of the effective potential $g^{\wedge}_{\lambda}(l l')$. This geometric factor $g^{\wedge}_{\lambda}(l l')$ represents the effective coupling between the positron angular momenta and the electronic angular anisotropy of the charge distribution of the molecule. Thus, in the BFVCC equation this geometric factor acts dynamically during the scattering processes. On the other hand, the BFVCC-AAMC's coupled differential equations (13) and (14) show that in this approximation the angular momentum of the positron is no longer coupled via the full effective potential of Eq. (5b) and therefore we are now obtaining radial scattering solutions that are uncoupled with respect to the angular momenta that are, in turn, treated as

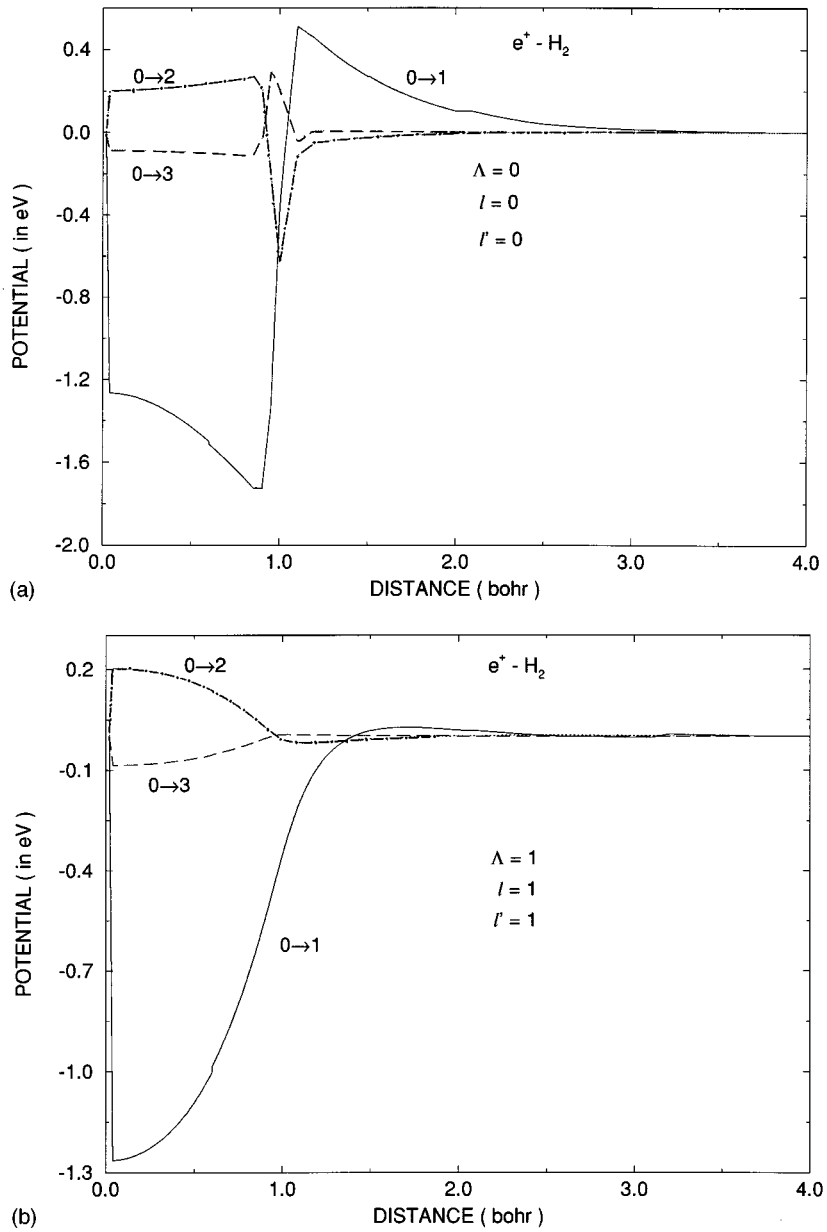

FIG. 1. Computed coupling potentials between vibrational states of H_2. Top, transitions form $v=0$ into $v'=1,2,3$ for the $\wedge=0$, $l=l'=0$ components, in eV. Bottom, same transitions for the $\wedge=1$, $l=l'=1$ components.

separate constants of motion. However, one still has the vibrationally coupled equation as in the BFVCC treatment discussed before. The effect of the geometric factor $g\hat{}_L(ll_0)$ on the scattering cross section appears now to be modified in the BFVCC-AAMC's scheme and does not act dynamically during the actual collision process but only in an adiabatic way by remaining fixed during each trajectory. In summary we could say that in the BFVCC scheme the vibrational motion of the nuclei, via the electronic motion of the molecule, is dynamically coupled to the motion of the positron while in the BFVCC-AAMC's approximation only the vibrational motion remains still coupled dynamically to the motion of positron. The complex recoupling of angular momenta between the molecule and the projectile is now treated instead adiabatically for each l value [14]. A comparison of the results using these two different coupling schemes can help us to better estimate the strength of the effect of the vibrational motion of the nuclei and the coupling strength of the rotational motion of the molecule on the positron dynamical angular momentum.

III. COMPUTATIONAL RESULTS

The present calculations were carried out for the H_2 and N_2 molecules, for which various earlier results, and their comparison with measurements, have been obtained before using the FNA decoupling scheme [18]. The target wave functions were obtained from Slater-type orbital (STO's) and Gaussian-type orbital (GTO's) basis set expansions, using the self-consistent field (SCF) results of Ref. [20] for the H_2 molecule and computing new GTO expanded SCF wave functions for the N_2 molecule [21]. The considered nuclear geometries were appropriate to include target vibrational levels up to $v=4$ for both molecules, i.e., involved an energy span of 1.88 eV for H_2 and of 1.13 eV for N_2. The ensuing static interaction, in its single-center-expansion (SCE) form, included $\lambda_{max}=22$ for H_2 and $\lambda_{max}=26$ for N_2 and the corresponding symmetries for the scattering positron that were kept in its expansion went up to $|\wedge|=4$, g and u components, for both systems. The correlation-polarization interaction V_{cp} was further taken into account by using a density functional

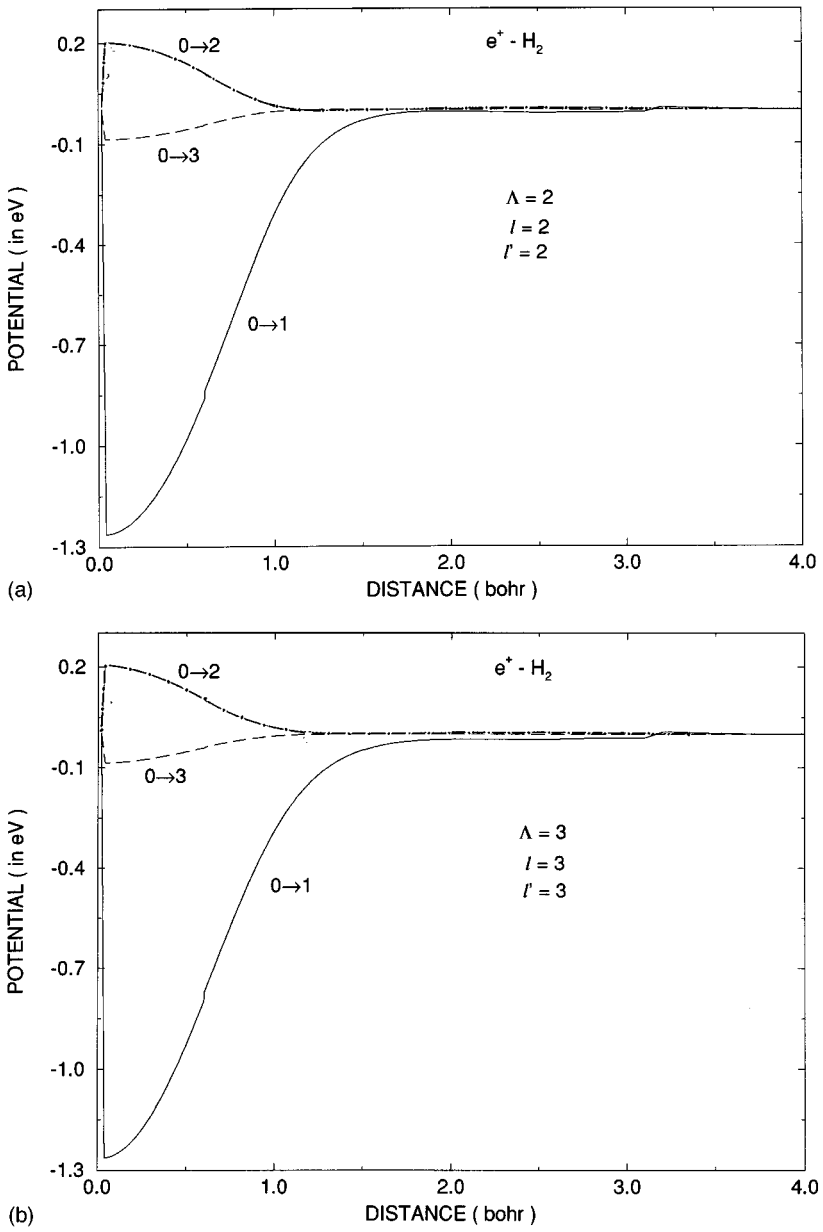

FIG. 2. Same as in Fig. 1 for different $\wedge$ states. Top, $\wedge=2$; bottom, $\wedge=3$. The components are $l=l'=2$, above, and $l=l'=3$, below; potentials are in eV and r_p distances are in bohr.

model for short-range dynamical correlation effects [9,18] and the perturbation expansion dipole polarizability coefficients in the long-range region. The actual de-tails of the method have been discussed before [18] and we will therefore not repeat them here. Suffice it to say that we have employed the version of the V_{cp} interaction that was modified for positron projectiles (and called these PCOP) and gave reasonable results for atomic and molecular targets [18,19]. The ensuing coupled equations included an expansion of positron partial waves up to $l_{max}=15$ for H_2 and up to $l_{max}=17$ for N_2. Thus, the coupled equations to be solved [Eq. (4)] went up to a maximum of 40 for H_2 and of 45 for N_2. In the integration radial range r_{max} was equal to $110a_0$ for H_2 and to $190a_0$ for N_2 and the equations were solved by numerical quadrature of the corresponding Volterra equations [9,18].

It is certainly instructive at this point to observe the behavior of the coupling vibrational matrix elements described in Eq. (5) over their radial range of action. As an example of this we present in Fig. 1 the general shape of the $\Lambda=0$ and 1 (top and bottom in the figure) coupling potentials between the initial vibrational level ($v=0$) and the excited levels with $v=1$, 2, and 3. The same coupling matrix elements for $\Lambda=2$ and $\Lambda=3$ are shown in Fig. 2, in both cases for the H_2 mo--lecular target. The same potential couplings are shown for the N_2 molecule in Figs. 3 and 4.

For both targets we can see the following. (i) The $\Delta v=1$ couplings ($0\rightarrow1$ transition) invariably show the strongest effects across the whole radial range in which they act. The couplings between levels with $\Delta v>1$ are invariably smaller and die much faster as $\mathbf{r}_p$ increases. (ii) The couplings for $\Lambda=0$ also show (in the $0\rightarrow1$ case) the presence of a strong barrier in the region just outside the nuclei, above $\approx1.0a_0$ from the center-of-mass position, while the $\Lambda=1$ components show a much smaller effect. No higher Λ contributions, however, show the presence of such strong effect. (iii) The coupling strength for the H_2 molecule is found to be always smaller than that for the N_2 target, a feature that will effect the final cross sections, as we shall see below.

In other words, what we see from the above comparison is

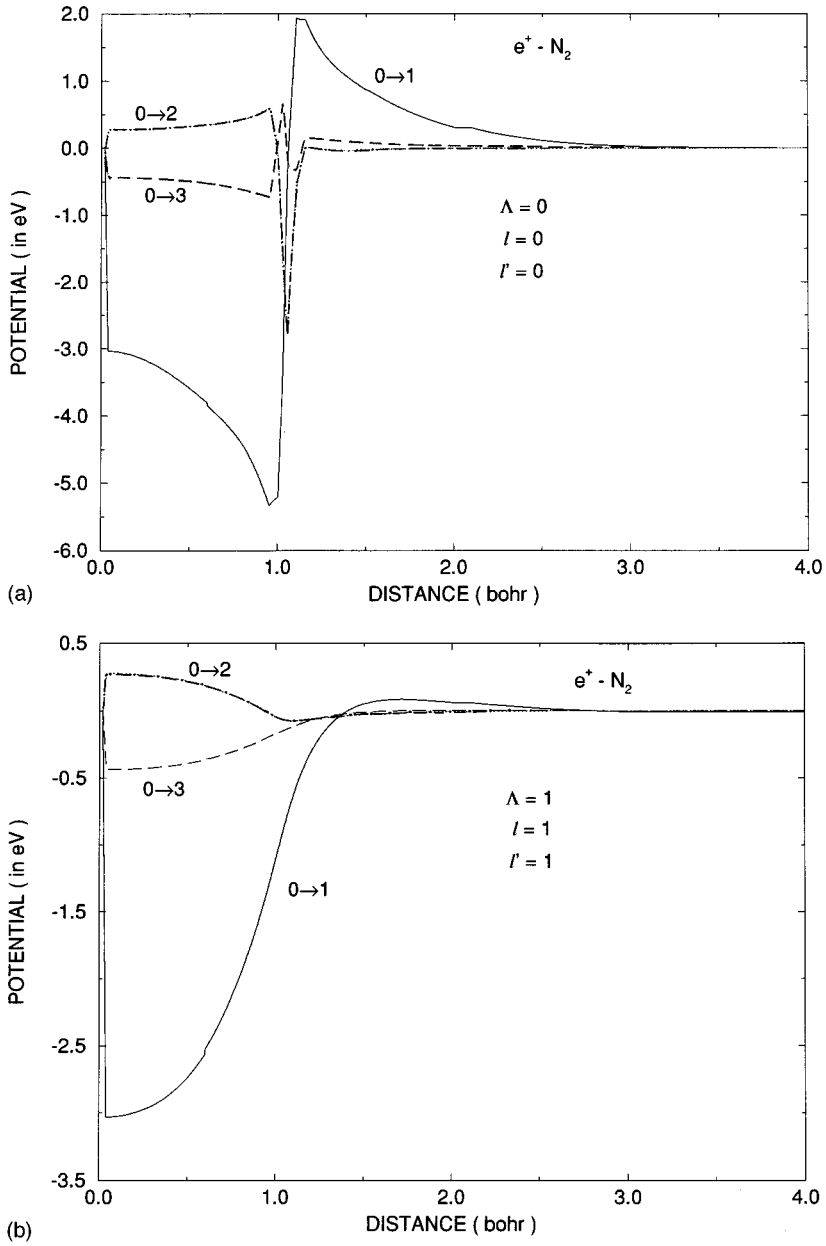

FIG. 3. Same as in Fig. 1 but for the N_2 system. Top, $\wedge=0$ component; bottom, $\wedge=1$ component.

the presence of a vibrational coupling that is at its strongest for the $(0\rightarrow1)$ excitation, that acts over a rather limited range of positron distances from the target and that is stronger in the case of N_2 molecules than in that of the H_2 target.

The direct consequences of the relative strength of the coupling is shown by the computed partial integral cross sections reported in Fig. 5. The upper part of the figure shows the BFVCC results for the H_2 molecule. The coupled equations were also solved retaining up to three closed vibrational channels above threshold and they are to be considered numerically converged within 1% of their values. We see there the following behavior. (i) The $(0\rightarrow1)$ excitation process is, as suggested earlier by the coupling potentials, by far the one with the largest cross section over the whole range of examined energies. The cross sections associated with transitions to higher levels are much smaller and decrease as the Δv value increases. (ii) The low-energy behavior of the partial cross section for the $(0\rightarrow1)$ excitation also shows a rather marked maximum for about 0.5 eV above the onset of its relative threshold. By repeating the calculations without any coupled channel the overall shape of that cross section does not change, thus indicating that we are not dealing here with Feshbach-type resonances [22] but with open-channel resonances induced by the shape of the effective potential. If we observe the coupling potential of Fig. 1 we see, in fact, that the barrier created by it outside the H position ($\approx0.7a_0$) is about 0.5 eV high for $l=0$ and may be able to trap the lower partial waves behind it, thereby increasing the efficiency of the vibrational energy transfer process.

A rather similar trend is observed in the case of the N_2 molecule, reported in the lower part of Fig. 5. We see first that the $(0\rightarrow1)$ inelastic cross section is here larger than in the case of H_2 but still very small: the coupled potential of Fig. 3 is in fact stronger, thus explaining this effect. The transitions with $\Delta v>1$, on the other hand, are again much smaller than the $(0\rightarrow1)$ cross sections but still larger for the N_2 molecule than for the H_2 target. Furthermore, the stronger barrier in the coupling of Fig. 3 affects now the $(0\rightarrow1)$ cross

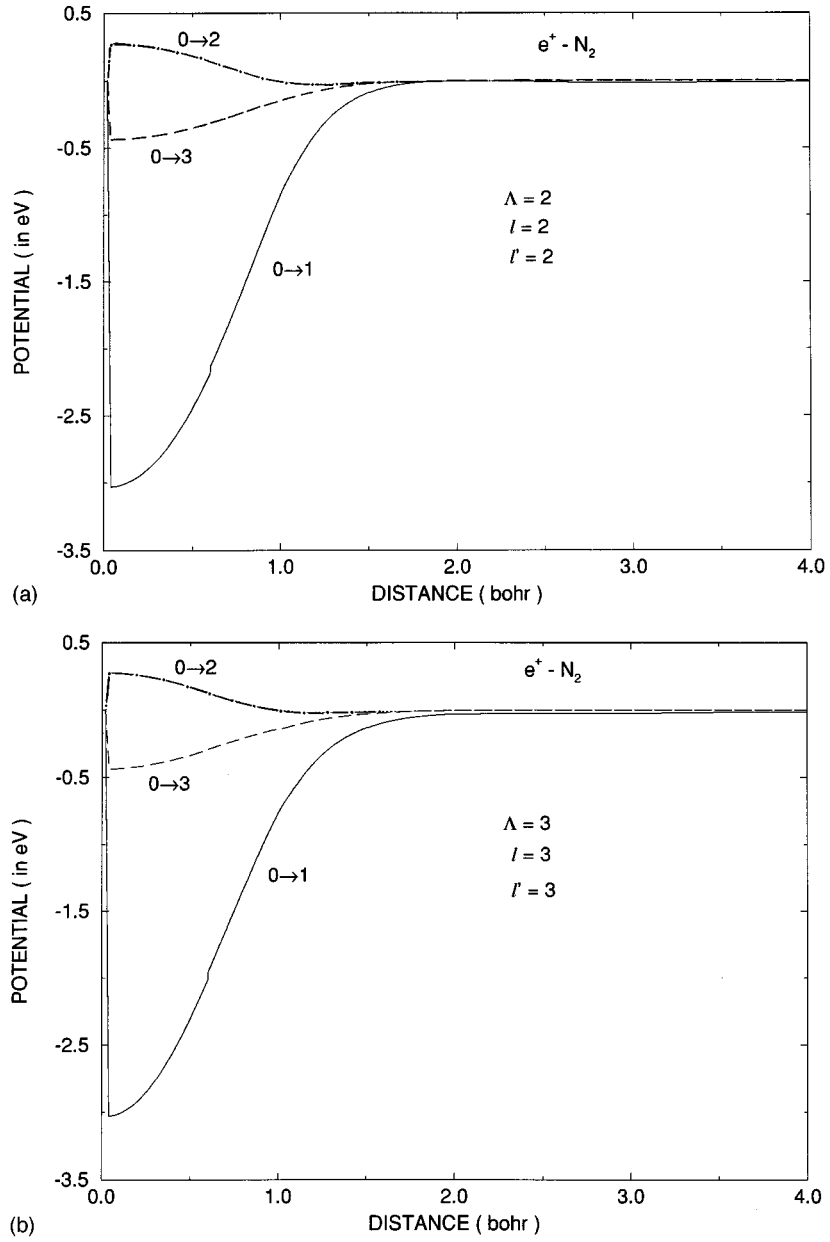

FIG. 4. Same as in Fig. 2 but for the N_2 system. Top, $\wedge=2$ component; bottom, $\wedge=3$ component.

section even more markedly. The height of the barrier is around 2 eV and we see that only beyond about 2 eV above threshold that excitation cross section decreases after a broad resonant maximum. Here again the maximum is unchanged by eliminating the closed channels and suggests therefore a resonant effect due to the actual shape of the coupling potentials.

We have mentioned in the Sec. II that the BFVCC calculations could be simplified by resorting to a BF form of the RIOS approximation discussed in the context of heavy-particle scattering [23]. In that case, the scattering equations were solved at a fixed orientation of the potential and the coupling between angular momenta was reduced to a sum over separate, adiabatic solutions for each of the contributing partial waves. Thus, the strength of the vibrational coupling was kept correctly for the potential part while its angular momentum coupling factor [Eq. (5b)] was strongly simplified as in Eq. (17).

The effects of such simplification on the final, state-to-state integral cross sections are shown by the results presented in Fig. 6. We report there the inelastic cross sections for H_2 in the upper part and for N_2 in the lower part of the figure.

If we analyze first the results for the H_2 target we see that the $(0\rightarrow1)$ cross section is already markedly different from the one reported in Fig. 5, obtained there with the correct BF angular momentum couplings. The lack of interference terms now makes the cross sections much larger, both at threshold and over the whole range of examined energies. The other excitation cross sections with $\Delta v>1$ are also much larger than before but still follow the qualitative behavior of decreasing in magnitude as Δv increases.

Another difference in behavior between the above cross sections and the BFVCC cross section is given by the appearance of strong oscillatory structures near the thresholds of each state-to-state cross section. This effect is possibly due to the artificial importance of potential barriers caused by the adiabatic decoupling: for about 0.5 eV above thresh-

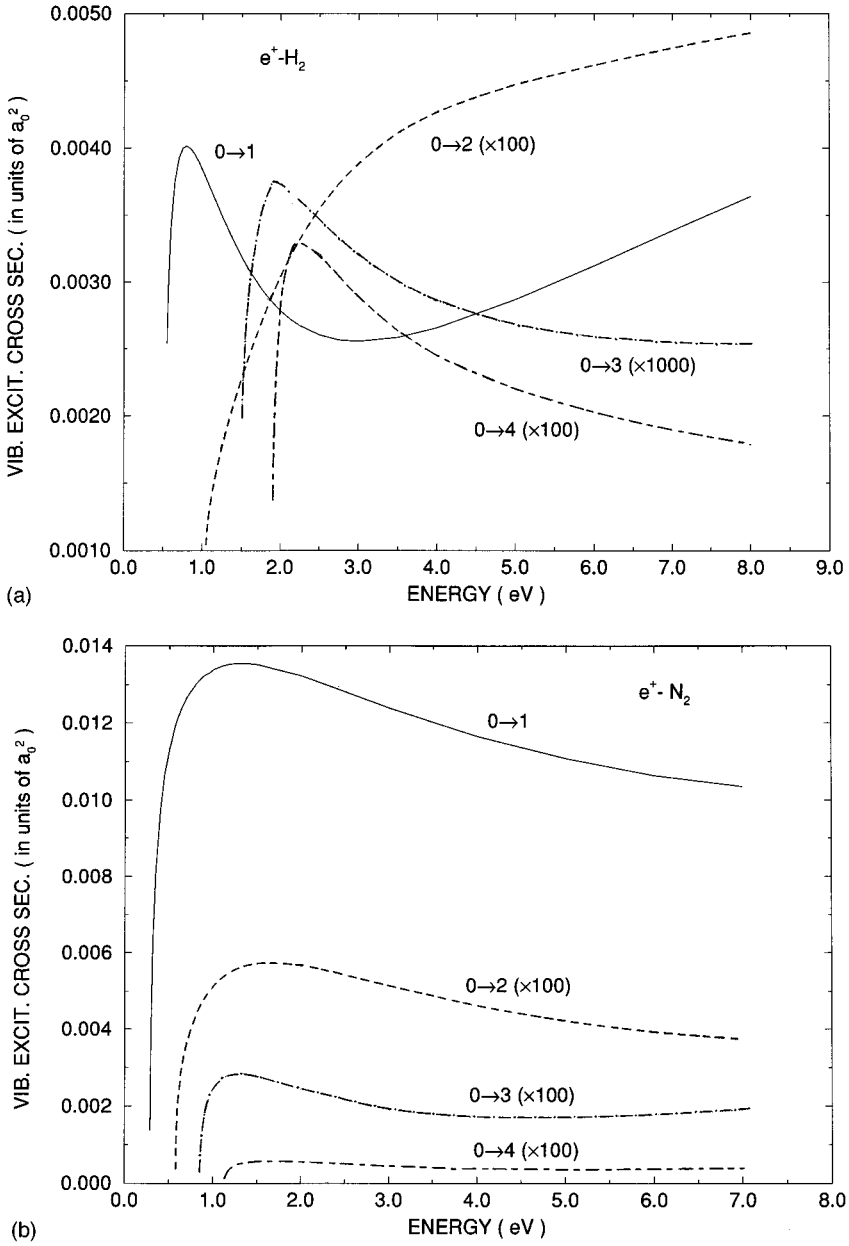

FIG. 5. Computed BFVCC vibrationally inelastic state-to-state cross sections. Top, for the H_2 molecule; bottom, for the N_2 molecule. The transitions with $\Delta v > 1$ are multiplied by the factors of 10 shown in brackets near each of them.

old the $(0\rightarrow 1)$ cross sections are able to be increased by shape resonances from each of the adiabatic l_0 values without being washed out by the interference terms included in Eq. (5b) within the BFVCC approach. Thus, the simplified angular coupling incorrectly enhances the importance of potential-dominated effects when the contributing angular momenta are treated separately.

This artifact from the RIOS decoupling is seen even more clearly in the results given by the vibrationally inelastic cross sections for the N_2 target (lower part of Fig. 6). The oscillatory structures in the $(0\rightarrow 1)$ and the $(0\rightarrow 2)$ cross sections now extend for about 1 eV above thresholds and give rise to many more oscillations than in the case of H_2. This is due both to the increased strength of the coupling vibrational potentials in this molecule and to the larger number of partial waves that contribute to this scattering process, as a consequence of the higher anisotropy of the target potential terms.

As a result of the reduced coupling, however, the BFVCC-AAMC's approximation appears to increase the inelastic processes since it considers the potential coupling a dominant contribution over the dynamical effects from angular momentum coupling between the molecule and the impinging positron.

Such differences in behavior can also be seen from the differences in value of a quantity defined as the average vibrational energy transfer

$$\langle \Delta E_v \rangle_{v=0} = \frac{\sum_{v\neq 0}^{v'} \sigma(v\rightarrow v')\Delta\varepsilon_{vv'}}{\sum_{v=0}^{v'} \sigma(v\rightarrow v')}, \tag{18}$$

which describes, from a given initial level, the overall probability of transferring energy into the molecular degrees of freedom by the impinging positron. In the present example,

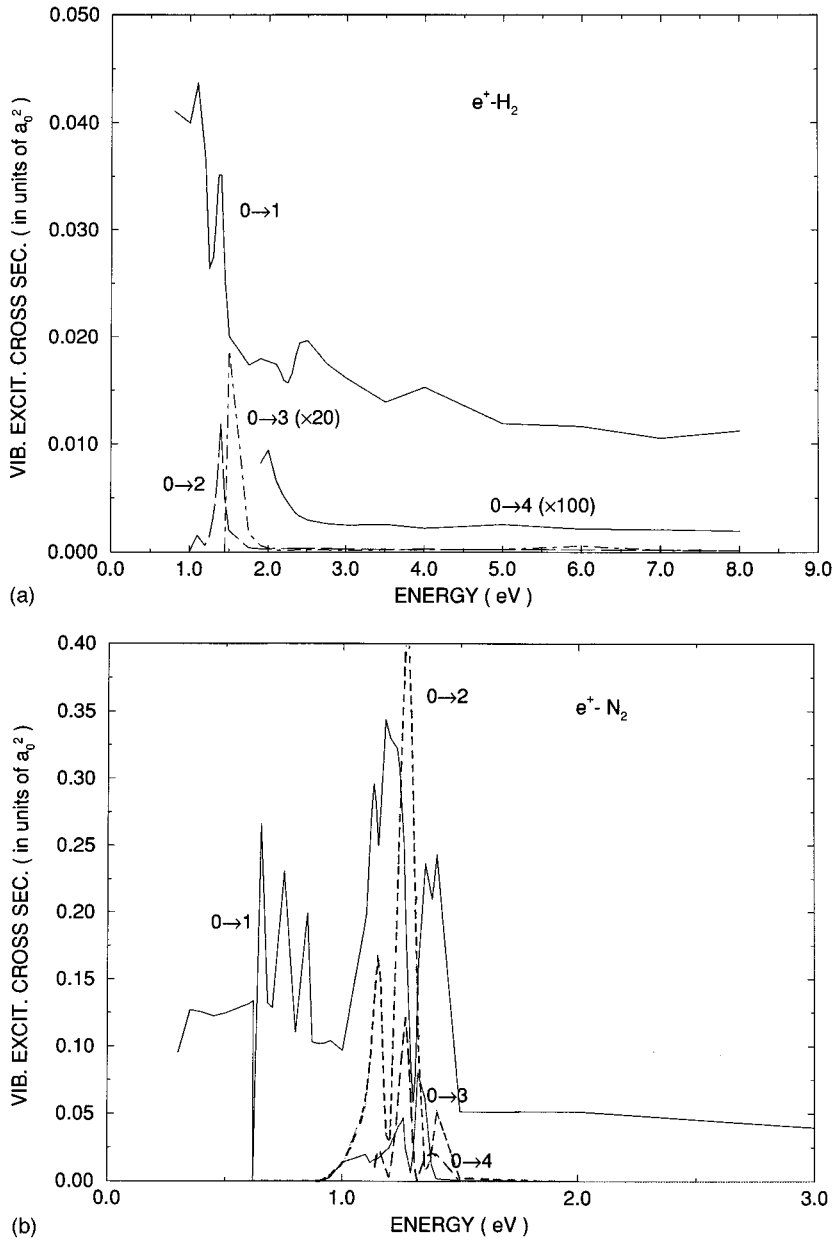

FIG. 6. Computed state-to-state inelastic cross sections using the AAMC scheme described in the main text. Top, H_2 molecule; bottom, N_2 molecule.

since no experiments are available, we consider the case in which the initially populated level is the $v=0$.

We report in Fig. 7 the results of the present calculations. The top diagrams refer to the H_2 molecule while the lower diagrams are for the N_2 molecule. The solid lines report the $\langle \Delta E_v \rangle$ values from the BFVCC calculations for both systems.

In the case of the hydrogen molecule we see that the amount of the energy transfer is rather small over the whole range of collision energies: in spite of the large values of the $\Delta\varepsilon_{vv'}$ energy gaps (e.g., 1.88 eV for the $\Delta\varepsilon_{04}$) the transfers are only of the order of meV, due to the small values of the inelastic cross sections. Their trend as a function of energy is to steadily increase from threshold up to $\approx$8.0 eV but never to go above $\approx$0.6 meV. The corresponding decoupled results (dotted line) are again very different and reflect the strong oscillations seen in the cross sections from Fig. 6. They are also larger on the average but follow a similar trend with energy.

The corresponding results for the N_2 molecule reflect the differences in structure between the two target systems. We see, in fact, in the lower part of Fig. 7 that the BFVCC calculations yield larger values for the $\langle \Delta E_v \rangle$ than in the case of H_2: considering the smaller energy spacings in the N_2 molecule one clearly sees that the partial inelastic cross sections constitute a larger portion of the total scattering process in the latter molecule than in the former case. Furthermore, the presence of low-energy shape resonances appears to affect the energy-transfer efficiency in the nitrogen target while it makes little difference for the H_2 system. The decoupled calculations produce the results shown in the inset of the lower part of Fig. 7. Here one sees that the artificial enhancement of resonant trapping given by the RIOS calculations drastically affects the efficiency for about 1 eV above threshold, while becoming comparable with the BFVCC results at higher collision energies.

Another interesting comparison is given by the calculations of the BFVCC total cross sections that can be compared with the experimental cross sections. Figure 8 reports

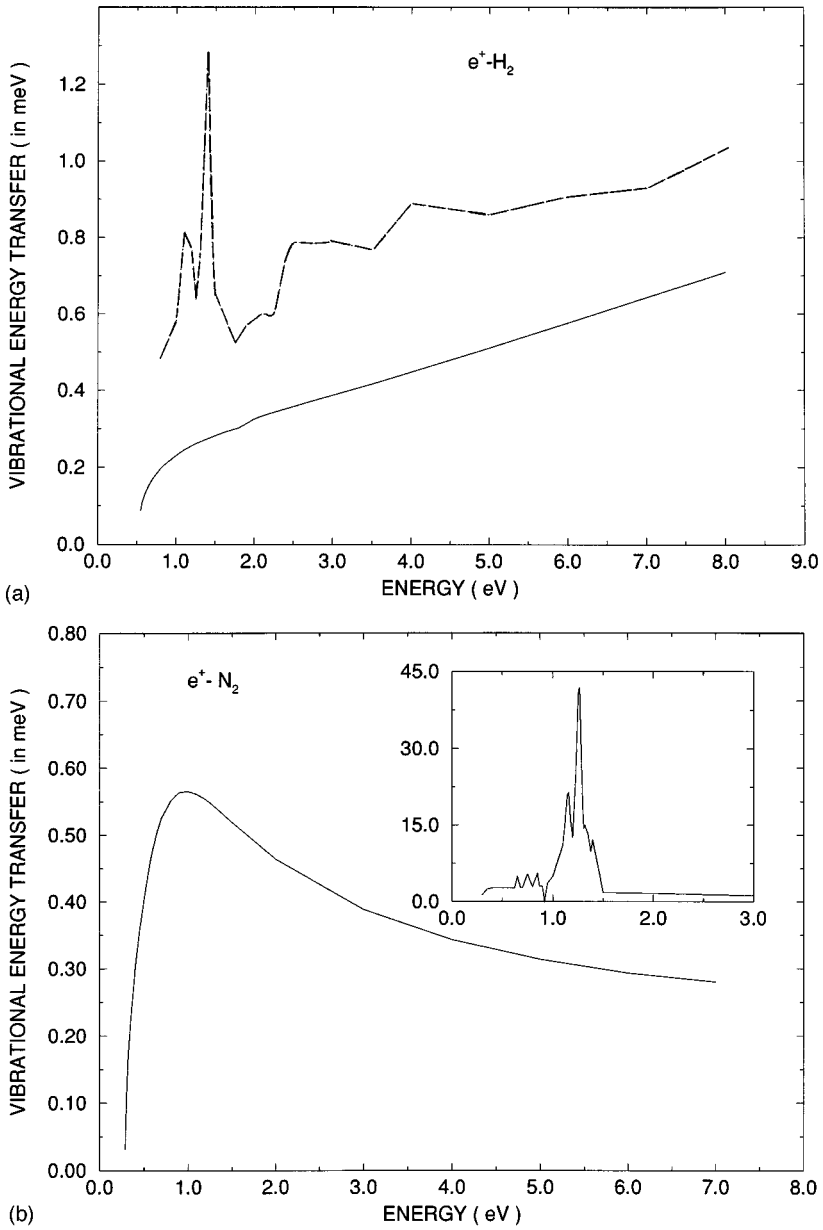

FIG. 7. Computed average vibrational energy transfer as defined by Eq. (18) in the main text. Top, H_2 molecule; bottom, N_2 molecule. The solid line refers to the BFVCC calculations while the dashed line (above) and the inset (below) refer to the decoupled AAMC scheme calculations. Quantities in meV and energy in eV.

such a comparison for the H_2 molecule. The experimental data are taken from Refs. [24, 25]. One sees that the BFVCC calculations agree rather well with measurements, especially as the collision energy increases. The inset in the figure reports more clearly the comparison and indicates that our present calculations indeed closely follow the measured data even below 1 eV of collision energy. On an enlarged scale, shown by the larger plot in the same figure, one can further compare the BFVCC calculations with those obtained using the AAMC's decoupling scheme (dotted curve). The latter results are too large at low collision energies and remain larger than the experiments over the whole range of examined energies. The only interesting feature is that the overall shape of the total cross section energy dependence follow rather closely the one given by the BFVCC results. It is also interesting to note that the present results constitute one of the best agreement obtained thus far between theory and experiments below the threshold of Ps formation [10,18].

A similar comparison between the present calculations and the experimental data is shown in Fig. 9 for the N_2 molecule. The measurements are taken from Refs. [24–26]. Once again we see that the BFVCC results (solid line) are in good agreement with the measurements, especially with that set of data that shows what appears to be as a Ramsauer-type minimum below 1 eV: our present calculations follow such data rather closely and reproduce well the low-energy cross section increase suggested by the experiments. The decoupled results from the AAMC calculations (dotted line) are again different from the more correct coupling but not as much as in the case of H_2: we see, in fact, that the two sets of calculations essentially agree with each other above 3 eV and differ for the more marked presence of the already discussed shape resonances in the region of energy between 0.5 and 2.0 eV in the case of the AAMC results. On the other hand, one could say that the two curves follow rather closely the same energy dependence and also the experimental findings. One should note at this point that the present calculations show among the best agreement with measurements found thus far by *ab initio* calculations and include for the

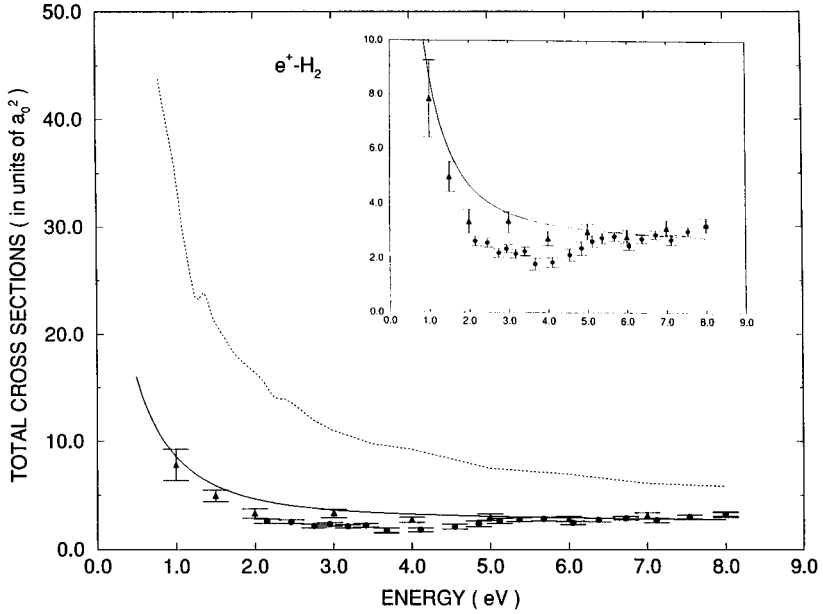

FIG. 8. Comparison between computed total integral cross sections and measured values for positron scattering off H_2. Solid line, computed BFVCC values; dotted line, decoupled AAMC's calculations. Experiments, filled triangles (from Ref. [24]); filled circles (from Ref. [25]). The inset shows only the comparison with the BFVCC calculations.

first time the contributions from vibrationally inelastic processes.

IV. GENERAL CONCLUSIONS

In the present study we have carried out close-coupled calculations of vibrationally inelastic processes in positron collisions with H_2 and N_2 molecules. The static and correlation-polarization interaction has been included via a local effective potential using PCOP modeling [18,19] and the coupling of the vibrational levels has been treated using two different schemes: the BFVCC equations described in Sec. II [12] and the decoupling scheme based on the IOS approximation, defined here as AAMC [Eq. (13)].

The results of the BFVCC calculations indicate the following.

(i) The excitation processes yield rather small cross sections over the range of examined energies indicating that, for both systems, positron projectiles are rather inefficient in ''heating'' the molecular gas.

(ii) The presence of shape resonances in the low-energy region above the $(0\rightarrow1)$ threshold enhances the σ_{01} process only over a rather small range of collision energies and is more effective for N_2 than for the H_2 target. The ensuing values of $\langle \Delta E_v \rangle$ the average energy-transfer indicator, are therefore more markedly affected for N_2 than for H_2.

(iii) The angular-momentum decoupling implied by the AAMC's approximation shows marked differences in the partial cross sections, both elastic and inelastic, and produces final, total integral cross sections which, for H_2, are too large when compared with measurements over the whole range of energies. On the other hand, the results for N_2 show that the two approaches are essentially the same above about 3 eV. Thus, one sees that the couplings between the positron angular momentum and that of the target via the strongly anisotropic interactions cannot be simplified as it can occur in the

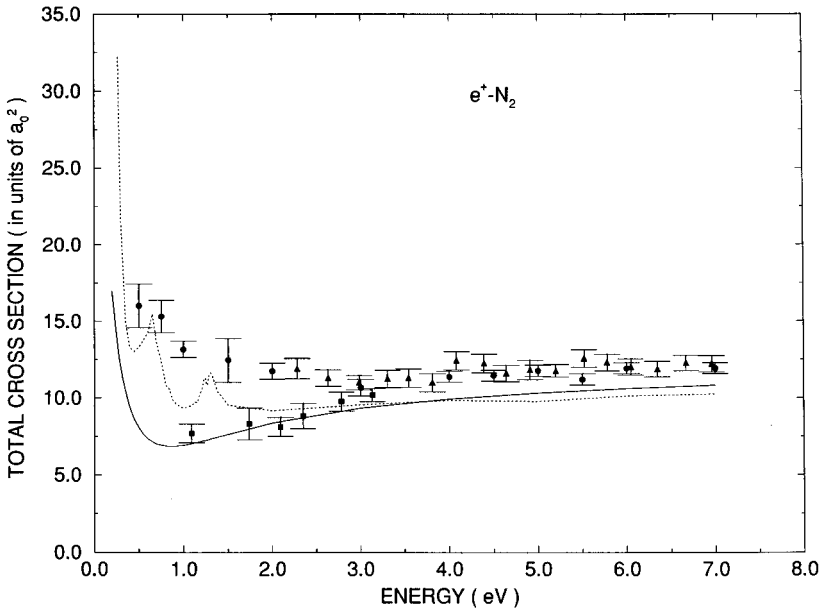

FIG. 9. Same as in Fig. 8 but for the N_2 molecule. The experiments are shown as filled circles (from Ref. [24]); filled squares (from Ref. [25]); filled triangles (from Ref. [26]).

case of the weaker van der Waals interactions for which such a method is usually suggested [27]. However, as the molecule becomes such that its density of vibrational states gets higher, we see that the two methods produce similar results especially with increasing energy.

(iv) The total cross sections that include the vibrational effects show rather good accord with the experimental data when the BFVCC coupling is employed and confirm the general validity of the present approach for treating correlation-polarization forces in closed-shell molecular systems interacting with positron [18,19]. A possible study of two- and three-photon annihilation rates might also provide a further test on the quality of the wave function obtained in this work [29], as it would also occur with the inclusion of the Ps formation channel.

An extension of the BFVCC calculations to CO and CO_2 systems is currently in preparation and will be reported elsewhere [28].

ACKNOWLEDGMENTS

The financial support of the Italian National Research Council (CNR) and of The Ministry for University and Research (MURST) is gratefully acknowledged.

[1] For example, see T. C. Griffith, in *Positron Scattering in Gases*, edited by J. W. Humbertson and M. R. C. McDowell (Plenum, New York, 1984).
[2] P. G. Coleman and J. T. Hutton, Phys. Rev. Lett. **45**, 2017 (1980).
[3] O. Sueoka, J. Phys. Soc. Jpn. **51**, 3757 (1982).
[4] M. Charlton, G. Clark, T. C. Griffith, and G. R. Heyland, J. Phys. B **16**, L465 (1983).
[5] T. S. Stein and W. E. Kauppila, in *Positron Annihilation*, edited by P. G. Coleman, S. C. Sharma, and L. M. Diana (North-Holland, Amsterdam, 1982).
[6] G. Laricchia and J. Moxom, Phys. Lett. A **174**, 255 (1993).
[7] A. Jain and D. G. Thompson, J. Phys. B **15**, L631 (1982).
[8] D. M. Schreder, Phys. Rev. A **20**, 918 (1979).
[9] F. A. Gianturco and P. Paioletti (unpublished).
[10] E. Armour, D. J. Baker, and M. Plummer, in *Electron-Molecule Scattering and Photoionization*, edited by P. G. Burke and J. B. West (Plenum, New York, 1987).
[11] M. A. Morrison, in *Positron (Electron)-Gas Scattering*, edited by W. E. Kauppila, T. S. Stein, and J. M. Wadehra (World Scientific, Singapore, 1986), p. 100.
[12] B. H. Choi and R. T. Poe, Phys. Rev. A **16**, 1821 (1977).
[13] M. A. Morrison, Aust. J. Phys. **36**, 239 (1983).
[14] P. Mc Guire and D. J. Kouri, J. Chem. Phys. **60**, 2488 (1974).
[15] P. Mc Guire, Chem. Phys. **4**, 483 (1974).
[16] R. T. Pack, J. Chem. Phys. **60**, 633 (1974).
[17] For example, see E. Buonomo, F. A. Gianturco, and F. Ragnetti, J. Phys. Chem. **100**, 9206 (1996).
[18] F. A. Gianturco, P. Paioletti, and J. A. Rodriguez-Ruiz, Z. Phys. D **36**, 51 (1996), and references quoted therein.
[19] F. A. Gianturco, A. Jain, and J. A. Rodriguez-Ruiz, Phys. Rev. A **48**, 4321 (1993).
[20] T. M. Dunning, J. Chem. Phys. **90**, 1007 (1989).
[21] F. A. Gianturco and F. Schneider, Mol. Phys. **89**, 753 (1996).
[22] R. G. Newton, *Scattering Theory of Waves and Particles* (Springer-Verlag, Berlin, 1982).
[23] For example, see F. A. Gianturco, *The Transfer of Molecular Energy by Collisions* (Springer-Verlag, Berlin, 1979).
[24] K. R. Hoffman, M. S. Dababneh, Y. F. Hsieh, W. E. Kauppila, U. Pal, J. H. Smart, and T. S. Stein, Phys. Rev. A **25**, 1393 (1982).
[25] M. Charlton, T. C. Griffith, G. R. Heyland, and G. L. Wright, J. Phys. B **16**, 323 (1983).
[26] O. Sueoka and S. J. Mori, J. Phys. Soc. Jpn. **53**, 2491 (1984).
[27] R. Parker and R. T. Pack, J. Chem. Phys. **6**, 1585 (1978).
[28] F. A. Gianturco and T. Mukherjee (unpublished).
[29] For example, see J. W. Humbertson, Adv. At. Mol. Phys. **22**, 1 (1986).